

# Prospects for independent measurement of $\ell=1,2,3$ CMB anisotropy multipoles using the anisotropic Sunyaev-Zel'dovich effect

D.I. Novikov, A.O. Mihalchenko, A.M. Osipova, K.O. Parfenov, and S.V. Pilipenko  
*Astro-Space Center of P.N. Lebedev Physical Institute, Profsoyusnaya 84/32, Moscow, 117997.*

We investigate the prospects for observing a specific spectral distortion of the cosmic microwave background, which occurs due to the anisotropy of the radiation when it is scattered by hot plasma of galaxy clusters. Detection of this 'anisotropic Sunyaev-Zel'dovich effect' will allow us to independently measure the anisotropy multipoles with  $\ell = 1, 2, 3$ , separate the Sachs-Wolf effect from the integrated Sachs-Wolf effect (Rees-Sciama effect) and, to a certain extent, circumvent the 'cosmic variance' problem for low multipoles. We propose a modified Least Response Method for the components separation in the data processing and estimate the required sensitivity of the experiment for such observations. We test our approach on a simulated signal that is contaminated by various foregrounds with poorly defined spectral shapes, along with distortions of the relic blackbody spectrum caused by the Sunyaev-Zel'dovich effect and its relativistic corrections.

PACS numbers:

Keywords: cosmic microwave background anisotropy, cosmology, spectral distortions, data analysis

## I. INTRODUCTION

Measurements of the cosmic microwave background (CMB) temperature anisotropy by WMAP [1] and Planck [2, 3] show alignment of the quadrupole and octupole [4–6] and a lack of power of multipoles with low  $\ell$  in the observed angular spectrum  $C_\ell$  [2, 7–9]. In addition, according to the studies [10–15] there are other large-scale anomalies in the temperature maps of the relic radiation. These facts are difficult to explain within the framework of Gaussian statistics and the inflationary model of the evolution of the Universe. Such anomalies may be due to incomplete removal of foreground components, particularly those from the Milky Way. As for the cosmological intrinsic dipole, it is completely overshadowed by our motion relative to the CMB rest frame. Besides, the observed anisotropy map represents only one realization of a random process, which inevitably leads to the 'cosmic variance' problem for low multipoles.

This suggests the need for an additional source of information about the low anisotropy multipoles, other than the CMB map that we directly observe. This source of information should not be so sensitive to the specific spatial distribution of foregrounds in our vicinity, should not depend on our motion relative to the CMB rest frame and should help us at least partially get around the 'cosmic variances' problem.

One possible way to obtain such alternative information on low multipoles is to observe the anisotropic Sunyaev-Zel'dovich effect (aSZ) described in [16, 17]. The influence of radiation anisotropy on the frequency spectrum as a result of scattering was also considered in [18]. This effect is a correction to the well known thermal Sunyaev-Zel'dovich effect (tSZ) [19, 20] due to the anisotropy of radiation scattered by hot electron plasma of galaxy clusters.

According to [21], the first correction to the Thomson scattering cross section is proportional to the electrons temperature  $\Theta_e = kT_e/m_e c^2$  and effectively depends on

the scattering angle. Using this fact, it was shown in [16, 17] that in the linear approximation in  $\Theta_e$  the dipole, quadrupole and octupole components of the anisotropic radiation incident on the cluster create a distinctive spectral distortion of the scattered radiation. The amplitude of this distortion is proportional to  $\sim \Theta_e \cdot \Delta T/T$ , where  $\Delta T/T$  is the anisotropy of the radiation at the scattering point. Thus, the isotropic monopole fraction of the radiation is responsible for the classical thermal effect, while the anisotropy of the radiation creates an additional anisotropic effect of a different spectral shape.

For an observer located in nearby clusters, the anisotropy map of the CMB should be roughly the same as in our location including the same in amplitude and orientation  $\Delta T/T$  multipoles with  $\ell = 1, 2, 3$ . Thus, observation of the relic radiation scattered on the nearby clusters with distorted frequency spectrum gives us a unique opportunity of an independent measurement of the CMB dipole, quadrupole and octupole.

As for distant clusters, according to [16, 17], observing such a distortion of the spectrum on a large number of clusters is a way to separate the Sachs-Wolfe effect (SW) [22] from the Integrated Sachs-Wolfe effect (ISW) [23] and to some extent get rid of the 'cosmic variance' for multipoles with  $\ell = 1, 2, 3$ . This is explained by the fact that the Integrated effect is formed at very low redshifts and, thus, the probe of the spectral distortions caused by the anisotropic SZ effect from high redshift SZ clusters is ISW-free.

In our article, we evaluate the practical possibility of detecting an aSZ signal in a real experiment. In this case, the multi-component nature of the observed signal must be considered, accounting for both relativistic corrections to the SZ effect and foreground signals of various origins.

Since the nineties of the last century, numerous studies have been published addressing various corrections of the Kompaneets equation [24] and SZ effect. Several relativistic corrections to the thermal SZ effect and multiple scattering on SZ clusters were considered in [25–33]. A

study of corrections for the kinematic SZ effect was carried out in [34–36]. An analytical investigation of the Boltzmann equations was made and expressions for the photon redistribution functions were conducted in [37–39]. The additional correction to the SZ signal due to the motion of the Solar System was discussed in [40]. The influence of the CMB anisotropy on the spectral distortions was investigated in [41–44].

The aforementioned studies show that the detecting the anisotropic SZ effect is puzzled by the need to separate it from other distortions associated with the Sunyaev-Zeldovich effect. Moreover, foreground signals, including galactic dust emission, the cosmic infrared background (CIB), synchrotron radiation, free-free emission, and potentially other sources, exceed the target signal by several orders of magnitude, significantly complicating observations and data analysis.

We consider a Fourier Transform Spectrometer (FTS) as a target instrument in our modelling. This kind of instruments are proven to be suitable for the study of CMB spectral distortions [45, 46]. In order to minimize foregrounds, the instrument should be placed in space [47–49].

Given the experiment’s limited sensitivity, a careful approach to data processing is especially important. Not only can this approach facilitate detection of the aSZ signal, but it can also enable separation of other components, revealing the diverse effects arising during the interaction of the CMB with the hot plasma of galaxy clusters. In addition, employing optimal data processing methods for PIXIE-like experiments [48, 50] enhances the detectability of  $\mu$  distortions [51–56] originating in the pre-recombination epoch.

The data processing approach must account for our poor knowledge of the expected spectra of some components (such as for example dust emission) whose parameters vary unpredictably along the line of sight.

In [57, 58] the Least Response Method (LRM) algorithm was developed for separating signals of interest from photon noise and foreground components with poorly defined spectra. Other known methods such as Internal Linear Combination (ILC) [59] and its modifications (cILC, mILC) [60–64] have proven to be insufficiently effective for our analysis. They either fail to remove foregrounds (ILC), or, having removed them all (mILC), fail to sufficiently suppress the contribution of photon noise. LRM minimizes the response to all foregrounds and noise simultaneously, leaving the response to the signal of interest constant. Unlike cILC or mILC, LRM does not require complete orthogonalization of the signal of interest to all other components, that is, the linear filtering of the observed signal across frequency channels does not completely cancel out the contribution from these components. This property mitigates the impact of photon noise. As a result, the desired signal can be detected with lower experimental sensitivity. Moreover, the LRM method can be modified to use an iterative approach to best estimate all signal components with well

defined spectral shapes (such as relativistic corrections to the SZ effect).

In our paper we apply a modified LRM for finding the aSZ signal in simulated data. The aim of this approach is to roughly estimate the required experimental sensitivity for aSZ observations and to test the mentioned multi-frequency data processing method. In this initial analysis we do not take into account the kinematic SZ effect and its relativistic corrections.

The paper is organized as follows: In Section II we review the anisotropic Sunyaev-Zel’dovich effect and describe foreground models, in Section III we review the LRM method and present its iterative modification for component separation. In Section IV we present our numerical results and finally in Section V we provide our brief conclusions.

## II. THE ANISOTROPIC THERMAL SZ EFFECT AND FOREGROUNDS

In this Section, we characterize (1) the spectral distortion generated by anisotropic radiation scattering off galaxy clusters as our signal of interest, and (2) the primary foreground components that challenge its detection.

### A. aSZ effect

To describe the anisotropic SZ effect we use the usual notations:  $I = I(\nu)$  is the spectral radiance, which is related to the photon number density as  $n(\nu) = \frac{c^2 I}{2h\nu^3}$ , where  $\nu, c, h$  are the frequency, the speed of light and the Planck constant respectively.  $T_e, T_r$  are the temperature of electrons and radiation,  $m_e$  is the rest mass of the electron,  $N_e$  is the concentration of electrons,  $\sigma_T$  is the Thomson cross section and  $\Theta_e = \frac{kT_e}{m_e c^2}$ , where  $k$  is the Boltzmann constant.

We consider the scattering of anisotropic radiation on a stationary cloud of hot electrons located within a galaxy cluster. The frequency spectrum of the radiation before scattering  $n_0(\nu)$  has a blackbody shape:

$$n_0(x) = B(x) = \frac{1}{e^x - 1}, \quad (1)$$

$$x = \frac{h\nu}{kT_r}.$$

We choose a local spherical coordinate system  $\Omega(\theta, \varphi)$  with the center at the scattering point and the north pole pointing to the observer. In this coordinate system, the temperature of the radiation incident on the cluster can be decomposed into spherical harmonics  $Y_{\ell m}$ :

$$T(\Omega) = \sum_{\ell m} \tilde{a}_{\ell m} \tilde{Y}_{\ell m}(\Omega). \quad (2)$$

Note, that  $\tilde{a}_{\ell m}, \tilde{Y}_{\ell m}$  are not the same as  $a_{\ell m}, Y_{\ell m}$  that belong to the conventional galactic coordinate system at our location.

In [16] it was shown that as a result of scattering in the optically thin limit and for  $T_r \ll T_e$ ,  $\Theta_e \ll 1$  the frequency spectrum distortion  $\Delta_n = n(x) - n_0(x)$  looks as follows:

The third term in Eq. (3) represents the classical thermal SZ effect (tSZ) for the isotropic fraction of radiation with the temperature  $T_r = \int T(\Omega) d\Omega$ , which corresponds to the monopole  $\ell = 0$  in Eq. (2), while the first two terms are due to the presence of CMB anisotropy. According to [16] only multipoles with  $\ell = 1, 2, 3$  distort the signal. The coefficients  $\gamma_1, \gamma_2, \gamma_3$  depend on the magnitude and orientation of the CMB dipole, quadrupole and octupole at the position of scattering:

$$\begin{aligned}\gamma_1 &= \frac{1}{4\sqrt{\pi}} \left( \frac{1}{\sqrt{5}} \tilde{a}_{20} - 2 \frac{\Delta_T(\Omega_z)}{T_r} \right), \\ \gamma_2 &= -\frac{3}{2\sqrt{\pi}} \left( \frac{2}{5\sqrt{3}} \tilde{a}_{10} + \frac{1}{\sqrt{5}} \tilde{a}_{20} - \frac{2}{5\sqrt{7}} \tilde{a}_{30} \right), \\ \gamma_3 &= -\frac{3}{4\sqrt{\pi}} \left( \frac{4}{5\sqrt{3}} \tilde{a}_{10} - \frac{1}{3\sqrt{5}} \tilde{a}_{20} + \frac{1}{5\sqrt{7}} \tilde{a}_{30} \right),\end{aligned}\quad (4)$$

where  $\Omega_z$  is the direction along the z-axis to the observer (to the north pole) and  $\Delta_T(\Omega) = T(\Omega) - T_r$ . It should be noted that the spectral distortions are produced only by the anisotropy of the incident radiation that is symmetrical relative to the z axis, i.e. by components with  $m=0$ .

The deviation of the form  $-x \frac{dB}{dx}$  [the first term in Eq. (3)] is of no interest to us since its shape coincides with the spectral variations caused by the observed temperature anisotropy. Indeed  $\frac{dB}{dT} = -\frac{x}{T} \frac{dB}{dx}$ . At the same time, the distortion  $\sim \frac{1}{x^2} \frac{d}{dx} [x^4 \frac{d}{dx} (-x \frac{dB}{dx})]$  [the second term in Eq. (3)] has a very characteristic spectral form, which allows us to separate it from other components of the observed signal. For convenience, in [16] this distortion was called the anisotropic SZ effect (aSZ). It is important to note that according to Eq. (3), the amplitudes of the anisotropic and thermal effects are both proportional to  $y_c \Theta$ . That is, the ratio of these amplitudes does not depend on the properties of the medium of the observed galaxy cluster. This makes it possible to directly estimate the coefficient  $\gamma_3$  when both effects are observed simultaneously. Thus, the component of the spectrum observed from a cluster of galaxies in the form of the aSZ effect is

considered as the signal of interest:

$$I_{asz}(\nu) = A_{asz} x \frac{d}{dx} \left[ x^4 \frac{d}{dx} \left( -x \frac{dB}{dx} \right) \right], \quad (5)$$

$$A_{asz} = \frac{2(kT_r)^3}{(hc)^2} y_c \Theta_e \gamma_3$$

Here,  $y_c \approx 1/100$ ,  $\Theta_e = 7.5 \text{ keV}/511 \text{ keV}$  and  $\gamma_3 \sim 5 \cdot 10^{-6}$ . Hence,  $A_{asz} \approx 0.2 \text{ Jy/sr}$ .

Considering the fact that the dipole, quadrupole and octupole contribute to the amplitude of the same frequency distortion, separating these contributions is only possible by measuring the spectrum from several clusters close to us, i.e., from clusters where these multipoles have the same fixed orientations and  $\Delta T/T$  amplitudes as at our location. In total, it is necessary to measure such a distortion from at least 15 clusters in order to separate the contributions from  $a_{\ell m}$ ,  $\ell = 1, 2, 3$ ,  $-\ell \leq m \leq \ell$  (from 3 dipole components, 5 quadrupole components and 7 octupole components). Using the expression for  $\gamma_3$  in Eq. (4), and also taking into account that  $a_{\ell m} \sim 1/\sqrt{\ell(\ell+1)}$  for low multipoles, one can estimate the magnitudes of the contributions from  $\ell = 1, 2, 3$  anisotropy to the overall effect:

$$A_{asz} = A_{asz}^{\ell=1} + A_{asz}^{\ell=2} + A_{asz}^{\ell=3}, \quad (6)$$

$$A_{asz}^{\ell=2}/A_{asz}^{\ell=1} \sim 0.19, \quad A_{asz}^{\ell=3}/A_{asz}^{\ell=1} \sim 0.07.$$

Therefore, the dipole component of the temperature anisotropy dominates this effect. Detecting the contribution from the octupole component requires significantly greater experimental sensitivity.

## B. Foregrounds

In our approach foregrounds are divided by their nature into two types: foregrounds with well defined spectral shapes and foregrounds with poorly defined spectra. Poorly defined spectra are parameterized spectra with floating parameters. However, these parameters can change only within a limited range of their possible variations. In addition, the amplitudes of all foregrounds cannot exceed certain pre-estimated values. Foregrounds with poorly defined spectra include dust emission, the cosmic infrared background (CIB) and synchrotron radiation.

Dust and CIB are considered together and modeled as a modified black body radiation with two floating parameters: temperature  $T$  and spectral index  $b$ :

$$\begin{aligned} I_{dust}(\nu, T_d, b_d) &= A_d(\nu/\nu_0)^{b_d} x_d^3 B(x_d), \quad x_d = \frac{h\nu}{kT_d}, \\ I_{CIB}(\nu, T_c, b_c) &= A_c(\nu/\nu_0)^{b_c} x_c^3 B(x_c), \quad x_c = \frac{h\nu}{kT_c}, \end{aligned} \quad (7)$$

where  $\nu_0 = 353$  GHz. The ranges of possible variations of  $T_d, b_d$  and  $T_c, b_c$  are shown in Fig. 1 (right panel) for relatively clean parts of the sky. The maximum allowable values for both  $A_d$  and  $A_c$  is estimated as  $3 \cdot 10^6$  Jy/sr.

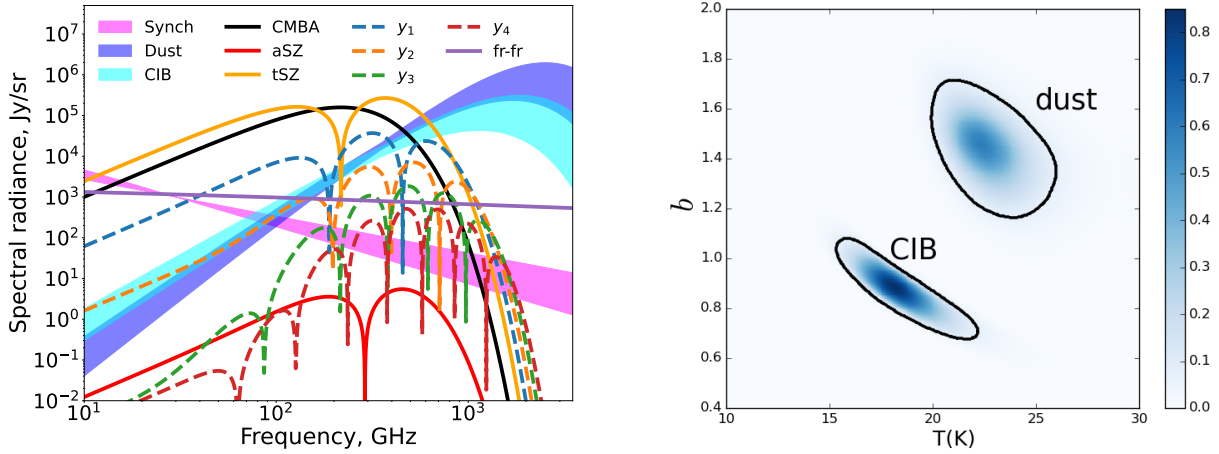


FIG. 1: *Left panel.* Spectra of the aSZ signal and main foregrounds. Emissions from dust, the CIB and the synchrotron are poorly defined spectra with floating parameters. Shaded areas show possible variations of these spectra. The remaining spectra have a strictly defined and well known shapes. *Right panel.* Probability distribution function of the  $T$  and  $b$  parameters for dust and CIB from the ‘cleanest’ regions of the sky. Isocontour lines limit the  $\tilde{\Omega}_1$  and  $\tilde{\Omega}_2$  regions of the parameter variations for dust and CIB respectively. The results are obtained from Planck data.

Synchrotron radiation is modeled according to [65, 66] and its spectrum is:

$$I_{sync}(\nu, b_s) = A_s(\nu/\nu_s)^{-b_s}, \quad (8)$$

where  $b_s$  is the only free parameter with possible variations  $0.9 \leq b_s \leq 1.4$ . Here  $\nu_s = 30$  GHz and  $A_s \approx 1000$  Jy/sr.

As foregrounds with well-defined spectra, we consider free-free emission and corrections associated with modifications of the blackbody spectrum of the relic radiation.

Free-free emission is given by the following formula [67]:

$$I_{ff}(\nu) = A_{ff} \left( 1 + \ln \left[ 1 + \left( \frac{\nu_{ff}}{\nu} \right)^{\sqrt{3}/\pi} \right] \right), \quad (9)$$

where,  $A_{ff} = 300$  Jy/sr,  $\nu_{ff} = 4728$  GHz. The parameter  $\nu_{ff}$  does not vary much across the sky to noticeably change the shape of the spectrum. Thus, in our calculations we consider free-free spectrum as well defined one.

Other foregrounds with well defined spectra include the CMB temperature anisotropy, which is the first derivative of  $B(x)$  with respect to radiation temperature  $T_r$ , and four relativistic corrections to the thermal SZ effect:

$$\begin{aligned} I_{CMBA}(\nu) &= A_{CMBA} x^4 \frac{dB}{dx}, \\ I_{y_0}(\nu) &= A_0 x \frac{d}{dx} \left[ x^4 \frac{dB}{dx} \right], \\ I_{y_n}(\nu) &= A_n \frac{x^4 e^x}{(e^x - 1)^2} Y_n(x), \quad n = 1, \dots, 4, \\ A_0 &= \frac{2(kT_r)^3}{(hc)^2} y_c \Theta_e, \quad A_n = A_0 \Theta_e^n \end{aligned} \quad (10)$$

where  $x = h\nu/kT_r$ ,  $T_r = 2.72548$  K, [68, 69]  $\Delta T/T_r < 10^{-4}$ ,  $A_{CMBA} \leq 3.24 \cdot 10^4$  Jy/sr,  $A_0 \approx 4 \cdot 10^4$  Jy/sr.

The functions  $Y_n(x)$ ,  $n \geq 1$  for the relativistic corrections have a rather cumbersome form and analytical formulas for them can be found in [70].

Another additional term in the observed signal is photon noise, which appears in each frequency channel as a random value. It comes from the CMB radiation, a number of main foregrounds and emission from the instrument including the optical system of the telescope. The magnitude of noise and its possible correlations between different frequency channels can be estimated in the process of observing the same galaxy cluster by subtracting from each other the signals observed at different times over the same time intervals.

The spectra of the foregrounds and the aSZ signal are presented in Fig. 1 (left panel).

### III. COMPONENTS SEPARATION USING A MODIFIED LEAST RESPONSE METHOD

The Least Response Method is a linear filtering of the observed signal that minimizes the response to all foregrounds and noise while keeping the response to the desired signal constant. It has the following distinctive features:

(1) It does not require complete orthogonalization of the various signal components. In other words, when determining the contribution of any component, this method does not completely cancel out the contributions of the remaining components with known spectra. This significantly mitigates the impact of photon noise on the calculation results. For example, if we have two components, one of which is significantly larger than the other, when finding the larger component, the LRM practically

ignores the smaller one, instead of setting it to zero and thereby increasing the response to white noise.

(2) It implies our knowledge of the limits of possible variation of the foreground spectral parameters for those foregrounds whose spectra are poorly defined.

### A. Least Response Method (LRM)

As shown in the previous Section, the observed frequency spectrum  $S(\nu)$  can be divided into two parts:

$$S(\nu) = I(\nu) + \tilde{I}(\nu), \quad (11)$$

where  $I(\nu)$  consists of components with well defined spectral shapes, while  $\tilde{I}(\nu)$  includes components with poorly defined spectra. In general, one can consider a total signal consisting of  $M$  components of different physical origin with well defined spectra and  $K$  components with poorly defined spectra:

$$I(\nu) = \sum_{m=1}^M I^m(\nu), \quad \tilde{I}(\nu) = \sum_{k=1}^K \tilde{I}^k(\nu). \quad (12)$$

Each component  $I^m(\nu)$  with a fixed spectral shape is described either by a known analytical function or by a strictly defined template  $f^m(\nu)$ :

$$I^m(\nu) = \alpha_m f^m(\nu), \quad m = 1, \dots, M, \quad (13)$$

where  $\alpha_m$  is the amplitude of the  $m$ -th component. Such components in the observed signal may include, for example, the thermal SZ effect, relativistic corrections to it or the anisotropic SZ effect.

When processing observational data using the LRM method, it is assumed that the amplitudes  $\alpha_m$  cannot exceed certain pre-estimated limits:

$$|\alpha_m| \leq A_m \quad m = 1, \dots, M. \quad (14)$$

Such upper limits on the amplitudes of various effects can be found from previous observations and numerical estimates.

As for components with poorly defined spectra, they can usually also be described by analytical functions  $\tilde{f}^k(\nu, \mathbf{P}_k)$ ,  $k = 1, \dots, K$ . Unlike well defined components, the shapes of their spectra depend on the set of parameters  $\mathbf{P}_k$  and change when these parameters are varied. One example of such a component is the emission of thermal dust. The uncertainty in the spectra arises from the integration of the signal along the line of sight, where the radiation from dust changes its parameters, such as temperature or the slope of the spectrum.

Similar to Eq. (13), the observed spectrum from such components can be written as follows:

$$\begin{aligned} \tilde{I}^k(\nu) &= \int_{\tilde{\Omega}_k} \tilde{\alpha}_k(\mathbf{P}_k) \tilde{f}^k(\nu, \mathbf{P}_k) d\mathbf{P}_k, \\ d\mathbf{P}_k &= dp_1^k dp_2^k \cdots dp_{L_k}^k, \quad k = 1, \dots, K, \end{aligned} \quad (15)$$

where  $\mathbf{P}_k = p_1^k, \dots, p_{L_k}^k$  is the set of  $L_k$  parameters of the  $k$ -th component and  $\tilde{\Omega}_k$  is the range of possible variations of these parameters.  $\tilde{\Omega}_k$  for each of the poorly defined components can be determined from the results of the previous experiments such as Planck and WMAP. Analogously to Eq. (14) we also assume that the amplitudes of the spectra  $\tilde{\alpha}_k$  are less than some pre-estimated values:

$$|\tilde{\alpha}_k(\mathbf{P}_k)| \leq \tilde{A}_k \quad \text{for } \mathbf{P}_k \in \tilde{\Omega}_k, \quad (16)$$

and  $\tilde{\alpha}_k(\mathbf{P}_k) = 0$  otherwise. Therefore, we do not know the exact shapes of the frequency spectra  $\tilde{I}_k$  that contribute to the overall observed spectrum, but only the limitations determined by Eq. (15, 16) on the signal they create.

During the observations we will observe a discrete signal  $S_j$  in  $J$  frequency channels  $\nu_j$ , consisting of the following terms:

$$S_j = \sum_{m=1}^M \alpha_m f_j^m + \sum_{k=1}^K \tilde{I}_j^k + N_j, \quad j = 1, \dots, J, \quad (17)$$

where  $f_j^m = f^m(\nu_j)$ ,  $\tilde{I}_j^k = \tilde{I}^k(\nu_j)$  and  $N_j$  is the photon noise. For convenience, this equation can be written in vector form:

$$\begin{aligned} \mathbf{S} &= \mathbf{F} + \tilde{\mathbf{F}} + \mathbf{N}, \\ \mathbf{F} &= \sum_{m=1}^M \alpha_m \mathbf{f}^m, \quad \tilde{\mathbf{F}} = \sum_{k=1}^K \tilde{\mathbf{I}}^k, \end{aligned} \quad (18)$$

where bold symbols  $\mathbf{X}$  denote row vectors  $\mathbf{X} = (X_1 \dots X_J)$ . Here  $\mathbf{F}$  is the sum of components with well defined spectra,  $\tilde{\mathbf{F}}$  contains all foregrounds with poorly defined spectra and  $\mathbf{N}$  is the noise with zero mean and covariance matrix  $[C_{ij}] = \mathbf{C} = \langle \mathbf{N}^T \mathbf{N} \rangle$ .

Our task is to estimate with the best accuracy all the coefficients  $\alpha_m$  for components with well defined spectral shapes, leaving untouched the poorly defined part of the observed spectrum. That is, we need to find the vector  $\boldsymbol{\alpha} = (\alpha_1 \dots \alpha_M)$ . For each component number  $m$ , the LRM method finds the optimal row vector of weights  $\boldsymbol{\omega}^m = (\omega_1^m \dots \omega_J^m)$ . This vector ensures for linear filtering the unit response to this component:  $\boldsymbol{\omega}^m \mathbf{f}^{mT} = 1$  and a minimal response to all other components and photon noise. Thus, we can introduce a matrix of the size  $J \times M$  whose columns are represented by the components of the row vectors  $\boldsymbol{\omega}^m$ :

$$\mathbf{W} = (\boldsymbol{\omega}^{1T} \boldsymbol{\omega}^{2T} \dots \boldsymbol{\omega}^{M^T}) = \begin{pmatrix} \omega_1^1 & \omega_1^2 & \dots & \omega_1^M \\ \omega_2^1 & \omega_2^2 & \dots & \omega_2^M \\ \vdots & \vdots & \ddots & \vdots \\ \omega_J^1 & \omega_J^2 & \dots & \omega_J^M \end{pmatrix} \quad (19)$$

By multiplying the observed signal vector  $\mathbf{S}$  by the matrix  $\mathbf{W}$ , we obtain an estimate for the amplitude vector  $\boldsymbol{\alpha}$ :

$$\bar{\boldsymbol{\alpha}} = \mathbf{S} \mathbf{W} = \boldsymbol{\alpha} + \mathbf{R}, \quad (20)$$

where the components  $R_m$  of the vector  $\mathbf{R}$  are as follows:

$$R_m = \omega^m \left[ \sum_{m'=1}^M \alpha_{m'} (1 - \delta_m^{m'}) \mathbf{f}^{m'} + \tilde{\mathbf{F}} + \mathbf{N} \right], \quad (21)$$

$m = 1, \dots, M.$

In [58] it was shown that the best weights for each  $m$ -th component that minimize the vector  $\mathbf{R}$  are:

$$\begin{aligned} \omega^m &= \mathbf{f}^m \mathbf{D}^{-1} \cdot (\mathbf{f}^m \mathbf{D}^{-1} (\mathbf{f}^m)^T)^{-1}, \\ \mathbf{D} &= \Phi^m + \tilde{\Phi} + \mathbf{C}. \end{aligned} \quad (22)$$

Here  $\Phi^m = [\Phi_{ij}^m]$  and  $\tilde{\Phi} = [\tilde{\Phi}_{ij}]$  are the  $J \times J$  covariance matrices of the foregrounds with well defined and poorly defined spectra respectively. They are calculated as follows:

$$\begin{aligned} \Phi_{ij}^m &= \sum_{m'=1}^M A_{m'}^2 (1 - \delta_m^{m'}) q_{ij}^{m'}, \quad q_{ij}^{m'} = f_i^{m'} f_j^{m'}, \\ \tilde{\Phi}_{ij} &= \sum_{k=1}^K \tilde{A}_k^2 \tilde{q}_{ij}^k, \\ \tilde{q}_{ij}^k &= \frac{1}{V_{\tilde{\Omega}_k}} \cdot \int_{\tilde{\Omega}_k} \tilde{f}_i^k(\mathbf{P}_k) \tilde{f}_j^k(\mathbf{P}_k) d\mathbf{P}_k, \\ V_{\tilde{\Omega}_k} &= \int_{\tilde{\Omega}_k} d\mathbf{P}_k. \end{aligned} \quad (23)$$

As can be seen from Eq. (20, 21), for each component  $m$  the difference between its estimated amplitude  $\bar{\alpha}_m$  and its true value  $\alpha_m$  is determined by the response  $R_m$ . This response consists of the response to foregrounds  $R_m^{fgr}$  (which are considered to be all other components with  $m' \neq m$ ) and the response to photon noise  $R_m^{Noise}$ :

$$\begin{aligned} R_m &= R_m^{fgr} + R_m^{Noise}, \quad m = 1, \dots, M, \\ R_m^{fgr} &= \omega^m \left[ \sum_{m'=1}^M \alpha_{m'} (1 - \delta_m^{m'}) \mathbf{f}^{m'} + \tilde{\mathbf{F}} \right], \quad (24) \\ R_m^{Noise} &= \omega^m \mathbf{N}. \end{aligned}$$

In approaches such as cILC and mILC, the weights  $\omega^m$  are calculated with the strict condition of zeroing the response to all foregrounds  $R_m^{fgr} = 0$ . This leads to an extremely uneven distribution of the weights  $\omega_j^m$  and their large values. This significantly increases the response to photon noise  $R_m^{Noise}$ . LRM, on the other hand, optimally distributes the response to foregrounds and noise in such a way that their combined response is minimized.

It is important to note that by using this approach to find the amplitudes  $\alpha_m$ , we have safely used the upper possible estimate for all other amplitudes  $\alpha_{m'}$ ,  $m' \neq m$ . Below we will show that refining the values  $\alpha_m$  using iterations significantly improves the result.

## B. Modified LRM

According to Eq. (19, 22, 23), the elements of the matrix  $\mathbf{W}$ , as well as the vectors  $\omega^m$ , are determined by the

covariance matrices  $\tilde{\Phi}$ ,  $\mathbf{C}$  and  $\Phi^m = \Phi^m(A_1, \dots, A_M)$ ,  $m = 1, \dots, M$ . Thus, for brevity, one can write:

$$\begin{aligned} \mathbf{W} &= \mathbf{W}(A_1, \dots, A_M), \\ \omega^m &= \omega^m(A_1, \dots, A_M), \quad m = 1, \dots, M. \end{aligned} \quad (25)$$

For convenience, we introduce the following notations:

$$\begin{aligned} \mathbf{W}_n &= \mathbf{W}(A_1^n, \dots, A_M^n), \\ \omega_n^m &= \omega^m(A_1^n, \dots, A_M^n), \quad m = 1, \dots, M, \\ \Phi_n^m &= \Phi^m(A_1^n, \dots, A_M^n), \quad m = 1, \dots, M, \\ \mathbf{R}_n &= \mathbf{R}(A_1^n, \dots, A_M^n), \\ A_m^0 &= A_m, \quad m = 1, \dots, M, \end{aligned} \quad (26)$$

We can apply the weights  $\mathbf{W}_0 = \mathbf{W}$  to the signal  $\mathbf{S}_0 = \mathbf{S}$  as just the first iteration in the process of finding the amplitudes  $\alpha$ :

$$\bar{\alpha}_0 = \mathbf{S}_0 \mathbf{W}_0 = \alpha + \mathbf{R}_0, \quad (27)$$

where  $\bar{\alpha}_0 = (\bar{\alpha}_1^0, \dots, \bar{\alpha}_M^0)$  and the response vector  $\mathbf{R}_0 = (R_1^0, \dots, R_M^0) = \mathbf{R}$  is determined by Eq. (21). The values of the response vector components  $R_m^0$  can be easily estimated from the following inequality:

$$\begin{aligned} \langle (R_m^0)^2 \rangle &\leq \omega_0^m (\Phi_0^m + \tilde{\Phi} + \mathbf{C}) \omega_0^{mT} = (A_m^1)^2, \\ m &= 1, \dots, M \end{aligned} \quad (28)$$

This inequality is a direct consequence of the assumptions in Eq. (14).

Using the preliminary estimation of  $\bar{\alpha} \approx \alpha$  from Eq. (26), we can consider a new signal  $\mathbf{S}_1$  which is obtained by subtracting the corresponding spectra from the initial signal:

$$\mathbf{S}_1 = \mathbf{S}_0 - \sum_{m=0}^M \bar{\alpha}_m^0 \mathbf{f}^m. \quad (29)$$

Thus, the spectrum  $\mathbf{S}_1$  contains new smaller amplitudes of the spectra  $\mathbf{f}^m$ . These residual amplitudes can be estimated using the inequality in Eq. (28). Since  $\alpha - \bar{\alpha}_0 = \mathbf{R}_0$ , we have the following new signal:

$$\begin{aligned} \mathbf{S}_1 &= \sum_{m=1}^M (\alpha_m^0 - \bar{\alpha}_m^0) \mathbf{f}^m + \tilde{\mathbf{F}} + \mathbf{N}, \\ |\alpha_m^0 - \bar{\alpha}_m^0| &\leq A_m^1, \quad m = 1, \dots, M. \end{aligned} \quad (30)$$

Therefore, we can continue to refine the values of the amplitudes  $\alpha$  using an iterative process that looks as follows:

$$\begin{aligned} \bar{\alpha}_n &= \mathbf{S}_n \mathbf{W}_n, \\ \mathbf{S}_{n+1} &= \mathbf{S}_n - \sum_{m=0}^M \bar{\alpha}_m^n \mathbf{f}^m, \\ A_m^{n+1} &= [\omega_n^m (\Phi_n^m + \tilde{\Phi} + \mathbf{C}) \omega_n^{mT}]^{\frac{1}{2}}, \\ \bar{\alpha}_{n+1} &= \mathbf{S}_{n+1} \mathbf{W}_{n+1}, \\ \star &\star \star \star \star \star \star \star \star \end{aligned} \quad (31)$$

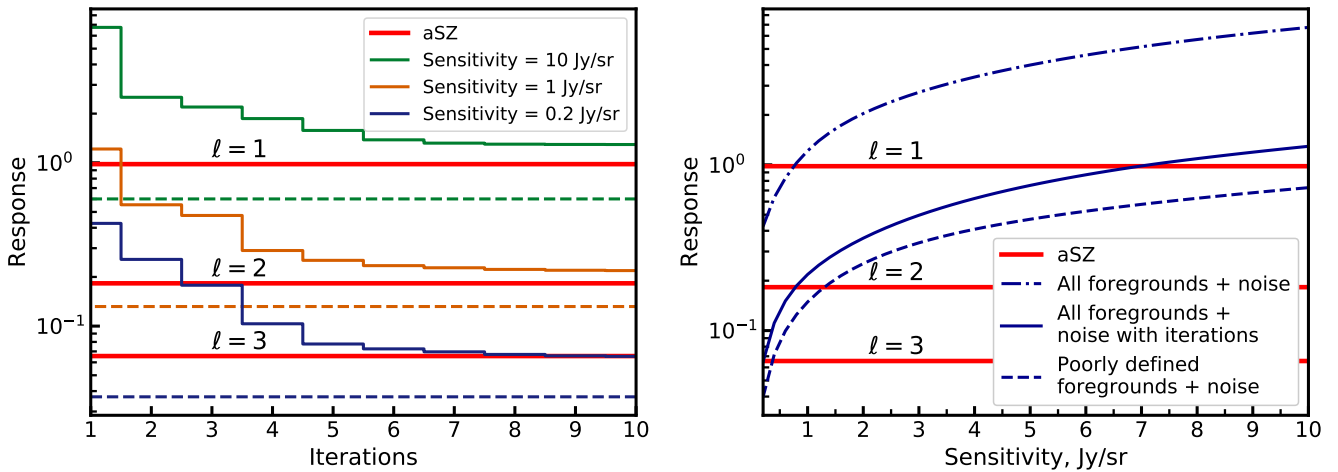


FIG. 2: Application of the LRM method and its iterative modification to extract the aSZ signal from the observed spectrum. *Left panel.* The solid stepped lines show the average response to all foregrounds and noise  $\sqrt{\langle (R_1^n)^2 \rangle}$  after each iteration  $n$  for different values of photon noise. Iteration with number  $n=1$  corresponds to the usual unmodified LRM method. The straight dashed lines correspond to the response to poorly defined foregrounds (dust+CIB+synchrotron) and noise. The red straight solid lines represent the response to the aSZ signal caused by the dipol ( $\ell = 1$ ) quadrupol ( $\ell = 2$ ) and octupol  $\ell = 3$  temperature anisotropy. *Right panel.* The solid blue line corresponds to the response to all foregrounds and noise after 10 iterations as a function of the photon noise (sensitivity). The upper dashed-dotted line shows the result of the conventional LRM method. The lower dashed line corresponds to the response to poorly defined foregrounds + noise. Red lines are the responses to the aSZ signal caused by multipoles with  $\ell = 1, 2, 3$ .

The iterations can be continued as long as the inequality  $|\bar{a}_m^n| \leq A_m^n$ ,  $m = 1, \dots, M$  remains valid. In the next Section we will show that this process converges in just a few iterations to values of amplitudes that are significantly smaller than the initially assumed  $A_m^0$ . In fact, using the iterations, we subtract from the observed spectrum most of the contribution from components with well defined spectra. As a result, the response to all foreground and noise becomes close to the response to only foregrounds with poorly defined spectra + noise:

$$R_m^n \approx \omega^m (\tilde{\mathbf{F}} + \mathbf{N})^T, \quad n \gg 1. \quad (32)$$

#### IV. NUMERICAL RESULTS

For the numerical analysis we use simulations of the signal passing along a single line of sight directed at a galaxy cluster with a plasma temperature of 7.5 KeV. The signal consists of discrete values  $S_j$ ,  $j = 1, \dots, J$  in  $J = 384$  frequency channels  $\nu_j$  covering the range from 10 GHz to 2.9 THz with a channel width of  $\Delta\nu = 7.5$  GHz. In accordance with the definitions and descriptions of foregrounds in Sections II and III, we consider 8 components whose spectral shapes are well defined ( $M = 8$ ), 3 components with poorly defined spectra ( $K = 3$ ) and photon noise.

The list of components looks as follows:

*Well defined spectra* ( $f^m(\nu_j)$ ):

- $m = 1$ : anisotropic SZ effect;
- $m = 2$ : thermal SZ effect;

$m = 3, 4, 5, 6$ : first four relativistic corrections to the thermal SZ effect respectively;

$m = 7$ : spectrum of free-free transitions;

$m = 8$ : spectrum of the CMB anisotropy.

Here we do not take into account the spectrum of the CMB monopole, since it can be easily removed from the observational data.

*Poorly defined spectra* ( $\tilde{f}^k(\nu_j, \mathbf{P}_k)$ ):

$k = 1$ : dust emission with 2 free parameters  $\mathbf{P}_1 = (T_d, b_d)$ ,  $\mathbf{P}_1 \in \tilde{\Omega}_1$ , see Eq. (7);

$k = 2$ : cosmic infrared background (CIB) with 2 free parameters  $\mathbf{P}_2 = (T_d, b_d)$ ,  $\mathbf{P}_2 \in \tilde{\Omega}_2$ , see Eq. (7);

$k = 3$ : synchrotron radiation with 1 free parameter  $\mathbf{P}_3 = b_s$ ,  $\mathbf{P}_3 \in \tilde{\Omega}_3$ , see Eq. (8).

Here the possible ranges of parameters variations  $\tilde{\Omega}_1, \tilde{\Omega}_2, \tilde{\Omega}_3$  are defined in Section II (see also Fig. 1).

*Photon noise:*

We model photon noise as white noise with a diagonal covariance matrix  $\mathbf{C} = \langle \mathbf{N} \mathbf{N}^T \rangle$ :  $C_{ij} = \delta_i^j \sigma^2$ . Here  $\sigma$  is the noise level per single channel. This value can be considered as the sensitivity of the experiment.

The results of our numerical experiment are shown in Fig. 2. We used the usual LRM method and its modification with iterations changing the sensitivity, i.e.  $\sigma$ . In both cases, we do not try to determine the contributions to the overall signal from poorly defined components, i.e. from the CIB dust and synchrotron, due to the lack of information about these spectra.

We are interested in the sensitivity needed to find the signal of interest, i.e. in this case the anisotropic SZ effect ( $m = 1$ ). The use of the simple LRM method

is equivalent to the first iteration in the modified LRM algorithm. It is easy to see that the modified approach converges in a small number of iterations  $n \sim 9$ . As a result of these iterations, the response to all remaining foregrounds and noise drops by approximately 8 times:  $R_1^9 \approx 1/8R_1^0$  (see also Eq. (32)).

In Fig. 2 we also show the response to only the poorly defined foregrounds and noise  $R_1(\mathbf{F}+\mathbf{N})$ . The iterations bring us close to this result as we got rid of most of the foregrounds with well defined spectra.

The modified LRM significantly improves the situation in terms of sensitivity or, in other words, in terms of the integrating time of observation required to accumulate the signal. As can be seen from Fig. 2 (left panel), a sensitivity of 7 Jy/sr is sufficient for the response to the aSZ signal, caused by the dipole anisotropy component, to be equal to the response to foregrounds and noise. For the quadrupole anisotropy, this is achieved with a sensitivity of  $\sim 1$  Jy/sr and for the octupole, with  $\sigma \sim 0.2$  Jy/sr.

## V. CONCLUSIONS

In our paper, we assessed the practical prospects for independent measurement of the CMB anisotropy multipoles with  $\ell = 1, 2, 3$  using the anisotropic Sunyaev-Zel'dovich effect.

Compared to the standard LRM method, our iterative modification demonstrates significantly improved capability to isolate the aSZ signal from other spectral components in galaxy cluster observations.

This method can be effectively applied to any observational data containing components with poorly defined spectra. One of the most promising areas to apply this approach apart from aSZ study, is the observation of  $\mu$  spectral distortions of the relic radiation.

We have not yet taken into account the kinematic SZ effect. Thus, our estimate of the sensitivity  $\sim 0.2$  Jy/sr to

detect the aSZ effect is not definitive and requires refinement. Adding the kinematic SZ effect and its relativistic corrections will increase the number of components that need to be separated from each other. However, it enables not only detection of CMB anisotropy at the scattering point, but also provides critical constraints on (1) the cluster plasma temperature, (2) the cluster's peculiar velocity relative to the CMB rest frame, and (3) its line-of-sight velocity component.

It is important to note that linear polarization occurs as a result of scattering of anisotropic radiation by clusters. The polarization produced as a result of 'cold' Thomson scattering in non-relativistic regime was considered in [71] for clusters at high redshifts to measure the CMB quadrupole and thereby getting around cosmic variance. Nevertheless the relic radiation itself is also initially polarized starting from the recombination epoch. Thus, without considering spectral distortions it is quite difficult to distinguish between the polarization resulting from scattering on the SZ cluster and the initial CMB polarization. In [17] it was shown that as a result of the aSZ effect, in addition to the distortion of the spectral radiance  $I(\nu)$ , a spectral distortion of the Stokes parameters  $Q(\nu)$  and  $U(\nu)$  arises as well. Unlike the spectral radiance, the spectrum of the Stokes parameters is distorted only by the quadrupole and octupole of the anisotropy. The dipole and, what is especially important, the CMB monopole do not introduce additional terms. This means that the relativistic thermal corrections from the dominant monopole do not contribute to the distortions of the polarization spectrum and the task of components separation is significantly simplified.

Thus, for further research it is necessary to include in the consideration the kinematic Sunyaev-Zeldovich effect and it is highly desirable to use the linear polarization of radiation coming from the galaxy cluster.

The work was supported by the RSF project (N 24-22-00230).

---

[1] C. L. Bennett, D. Larson, J. L. Weiland, N. Jarosik, G. Hinshaw, N. Odegard, K. M. Smith, R. S. Hill, B. Gold, M. Halpern, et al., *Astrophys. J., Supplement* **208**, 20 (2013), 1212.5225.

[2] P. A. R. Ade, N. Aghanim, C. Armitage-Caplan, M. Arnaud, M. Ashdown, F. Atrio-Barandela, J. Aumont, C. Baccigalupi, A. J. Banday, and et al. (Planck Collaboration), *Astron. Astrophys.* **571**, A15 (2014), 1303.5075.

[3] Planck Collaboration, Y. Akrami, M. Ashdown, J. Aumont, C. Baccigalupi, M. Ballardini, A. J. Banday, R. B. Barreiro, N. Bartolo, S. Basak, et al., *Astron. Astrophys.* **641**, A4 (2020), 1807.06208.

[4] C. J. Copi, D. Huterer, and G. D. Starkman, *Phys. Rev. D* **70**, 043515 (2004), astro-ph/0310511.

[5] C. J. Copi, D. Huterer, D. J. Schwarz, and G. D. Starkman, *Mon. Not. R. Astron. Soc.* **367**, 79 (2006), astro-ph/0508047.

[6] P. D. Naselsky and O. V. Verkhodanov, *Int. J. of Mod. Phys. D* **17**, 179 (2008), astro-ph/0609409.

[7] G. Efstathiou, *Mon. Not. R. Astron. Soc.* **346**, L26 (2003), astro-ph/0306431.

[8] M. Tegmark, A. de Oliveira-Costa, and A. J. Hamilton, *Phys. Rev. D* **68**, 123523 (2003), astro-ph/0302496.

[9] D. J. Schwarz, G. D. Starkman, D. Huterer, and C. J. Copi, *Phys. Rev. Lett.* **93**, 221301 (2004), astro-ph/0403353.

[10] C. J. Copi, D. Huterer, D. J. Schwarz, and G. D. Starkman, *Advances in Astronomy* **2010**, 847541 (2010), 1004.5602.

[11] S. Nadathur, M. Lavinto, S. Hotchkiss, and S. Räsänen, *Phys. Rev. D* **90**, 103510 (2014), 1408.4720.

[12] Y. Wang and Y.-Z. Ma, arXiv e-prints arXiv:1501.00282 (2015), 1501.00282.

[13] Planck Collaboration, P. A. R. Ade, N. Aghanim,

Y. Akrami, P. K. Aluri, M. Arnaud, M. Ashdown, J. Aumont, C. Baccigalupi, A. J. Banday, et al., *Astron. Astrophys.* **594**, A16 (2016), 1506.07135.

[14] D. J. Schwarz, C. J. Copi, D. Huterer, and G. D. Starkman, *Classical and Quantum Gravity* **33**, 184001 (2016), 1510.07929.

[15] J. Creswell and P. Naselsky, *Journal of Cosmology and Astroparticle Physics* **2021**, 103 (2021), 2102.13442.

[16] I. G. Edigaryev, D. I. Novikov, and S. V. Pilipenko, *Phys. Rev. D* **98**, 123513 (2018).

[17] D. I. Novikov, S. V. Pilipenko, M. De Petris, G. Luzzi, and A. O. Mihalchenko, *Phys. Rev. D* **101**, 123510 (2020).

[18] J. Chluba, D. Nagai, S. Sazonov, and K. Nelson, *Mon. Not. R. Astron. Soc.* **426**, 510 (2012), 1205.5778.

[19] Y. B. Zeldovich and R. A. Sunyaev, *Astrophys. Space. Sci.* **4**, 301 (1969).

[20] R. A. Sunyaev and Y. B. Zeldovich, *Astrophys. Space. Sci.* **7**, 20 (1970).

[21] J. P. Babuel-Peyrissac and G. Rouvillois, *Journal de Physique* **30**, 301 (1969).

[22] R. K. Sachs and A. M. Wolfe, *Astrophys. J.* **147**, 73 (1967).

[23] M. J. Rees and D. W. Sciama, *Nature (London)* **217**, 511 (1968).

[24] A. S. Kompaneets, *Sov. J. Exp. Theor. Phys.* **4**, 730 (1957).

[25] J. Chluba, R. Khatri, and R. A. Sunyaev, *Mon. Not. R. Astron. Soc.* **425**, 1129 (2012).

[26] J. Chluba, L. Dai, and M. Kamionkowski, *Mon. Not. R. Astron. Soc.* **437**, 67 (2014), 1308.5969.

[27] J. Chluba and L. Dai, *Mon. Not. R. Astron. Soc.* **438**, 1324 (2014), 1309.3274.

[28] A. Challinor and A. Lasenby, *Astrophys. J.* **499**, 1 (1998).

[29] N. Itoh, Y. Kohyama, and S. Nozawa, *Astrophys. J.* **502**, 7 (1998), astro-ph/9712289.

[30] A. Stebbins, Submitted to: *Astrophys. J. Lett.* (1997), astro-ph/9709065.

[31] M. Shimon and Y. Rephaeli, *Astrophys. J.* **575**, 12 (2002), astro-ph/0204355.

[32] N. Itoh, Y. Kawana, S. Nozawa, and Y. Kohyama, *Mon. Not. Roy. Astron. Soc.* **327**, 567-576 (2001), astro-ph/0005390.

[33] W. Hu, D. Scott, and J. Silk, *Phys. Rev. D* **49**, 648 (1994), astro-ph/9305038.

[34] S. Nozawa, N. Itoh, and Y. Kohyama, *Astrophys. J.* **508**, 17 (1998), astro-ph/9804051.

[35] S. Y. Sazonov and R. A. Sunyaev, *Astrophys. J.* **508**, 1 (1998).

[36] A. Challinor and A. Lasenby, *Astrophys. J.* **510**, 930 (1999), astro-ph/9805329.

[37] S. Nozawa and Y. Kohyama, *Phys. Rev. D* **79**, 083005 (2009), 0902.2595.

[38] S. Nozawa and Y. Kohyama, *Mon. Not. R. Astron. Soc.* **434**, 710 (2013), 1303.2286.

[39] S. Nozawa and Y. Kohyama, *Mon. Not. R. Astron. Soc.* **441**, 3018 (2014), 1402.1541.

[40] J. Chluba, G. Hütsi, and R. A. Sunyaev, *Astron. Astrophys.* **434**, 811 (2005), astro-ph/0409058.

[41] S. Yasini and E. Pierpaoli, *Phys. Rev. D* **94**, 023513 (2016).

[42] S. A. Balashev, E. E. Kholupenko, J. Chluba, A. V. Ivanchik, and D. A. Varshalovich, *Astrophys. J.* **810**, 131 (2015), 1505.06028.

[43] S. Yasini and E. Pierpaoli, *Physical Review Letters* **119**, 221102 (2017), 1610.00015.

[44] P. d. S. Ferreira and M. Quartin, *Phys. Rev. Lett.* **127**, 101301 (2021), 2011.08385.

[45] D. J. Fixsen, E. S. Cheng, J. M. Gales, J. C. Mather, R. A. Shafer, and E. L. Wright, *Astrophys. J.* **473**, 576 (1996), astro-ph/9605054.

[46] P. de Bernardis, S. Colafrancesco, G. D'Alessandro, L. Lamagna, P. Marchegiani, S. Masi, and A. Schillaci, *Astron. Astrophys.* **538**, A86 (2012), 1111.4588.

[47] I. D. Novikov, S. F. Likhachev, Y. A. Shchekinov, A. S. Andrianov, A. M. Baryshev, A. I. Vasyunin, D. Z. Wiebe, T. d. Graauw, A. G. Doroshkevich, I. I. Zinchenko, et al., *Physics Uspekhi* **64**, 386 (2021).

[48] A. Kogut, J. Chluba, D. J. Fixsen, S. Meyer, and D. Spergel, in *Space Telescopes and Instrumentation 2016: Optical, Infrared, and Millimeter Wave*, edited by H. A. MacEwen, G. G. Fazio, M. Lystrup, N. Batalha, N. Siegler, and E. C. Tong (2016), vol. 9904 of *Society of Photo-Optical Instrumentation Engineers (SPIE) Conference Series*, p. 99040W.

[49] J.-P. Maillard, *Philosophical Transactions of the Royal Society A: Mathematical, Physical and Engineering Sciences* **379**, 20200212 (2021).

[50] J. C. Hill, N. Battaglia, J. Chluba, S. Ferraro, E. Schaan, and D. N. Spergel, *Phys. Rev. Lett.* **115**, 261301 (2015), 1507.01583.

[51] R. A. Sunyaev and Y. B. Zeldovich, *Astrophys. Space. Sci.* **9**, 368 (1970).

[52] W. Hu and J. Silk, *Phys. Rev. Lett.* **70**, 2661 (1993).

[53] R. Khatri and R. A. Sunyaev, *Journal of Cosmology and Astroparticle Physics* **2012**, 016 (2012), 1207.6654.

[54] J. Chluba, A. L. Erickcek, and I. Ben-Dayan, *Astrophys. J.* **758**, 76 (2012), 1203.2681.

[55] J. Yang, X. Wang, X.-H. Ma, D. Zhang, S.-F. Yan, A. Ilyas, and Y.-F. Cai, *Phys. Rev. D* **111**, 043522 (2025).

[56] J. Mastache, W. Barrera, and R. Henríquez-Ortiz, *Journal of Cosmology and Astroparticle Physics* **2024**, 070 (2024), 2311.13737.

[57] D. I. Novikov and A. O. Mihalchenko, *Phys. Rev. D* **107**, 063506 (2023), 2303.07671.

[58] J. P. Maillard, A. Mihalchenko, D. Novikov, A. Osipova, S. Pilipenko, and J. Silk, *Phys. Rev. D* **109**, 023523 (2024), 2401.13415.

[59] G. B. Rybicki and W. H. Press, *Astrophys. J.* **398**, 169 (1992).

[60] M. Remazeilles, J. Delabrouille, and J.-F. Cardoso, *Mon. Not. R. Astron. Soc.* **418**, 467 (2011), 1103.1166.

[61] M. Remazeilles and J. Chluba, *Mon. Not. R. Astron. Soc.* **494**, 5734 (2020), 1907.00916.

[62] V. Stolyarov, M. P. Hobson, A. N. Lasenby, and R. B. Barreiro, *Mon. Not. R. Astron. Soc.* **357**, 145 (2005), astro-ph/0405494.

[63] J. Chluba, J. C. Hill, and M. H. Abitbol, *Monthly Notices of the Royal Astronomical Society* **472**, 1195 (2017), ISSN 0035-8711.

[64] A. Rotti and J. Chluba, *Monthly Notices of the Royal Astronomical Society* **500**, 976 (2020), ISSN 0035-8711.

[65] G. B. Rybicki and A. P. Lightman, *Radiative Processes in Astrophysics* (Wiley-VCH, 1986).

[66] E. de la Hoz, R. B. Barreiro, P. Vielva, E. Martínez-González, J. A. Rubiño-Martín, B. Casaponsa, F. Guidi, M. Ashdown, R. T. Génova-Santos, E. Artal, et al., *Mon. Not. R. Astron. Soc.* **519**, 3504 (2023), 2301.05117.

- [67] Planck Collaboration, R. Adam, P. A. R. Ade, N. Aghanim, M. I. R. Alves, M. Arnaud, M. Ashdown, J. Aumont, C. Baccigalupi, A. J. Banday, et al., *Astron. Astrophys.* **594**, A10 (2016), 1502.01588.
- [68] J. C. Mather, E. S. Cheng, J. Eplee, R. E., R. B. Isaacman, S. S. Meyer, R. A. Shafer, R. Weiss, E. L. Wright, C. L. Bennett, N. W. Boggess, et al., *Astrophys. J., Lett.* **354**, L37 (1990).
- [69] D. J. Fixsen, *Astrophys. J.* **707**, 916 (2009).
- [70] A. D. Challinor, M. T. Ford, and A. N. Lasenby, *Mon. Not. R. Astron. Soc.* **312**, 159 (2000).
- [71] M. Kamionkowski and A. Loeb, *Phys. Rev. D* **56**, 4511 (1997), astro-ph/9703118.